Plasmon damping below the Landau regime: the role of defects in epitaxial graphene

2010 New J. Phys. 12 033017

(http://iopscience.iop.org/1367-2630/12/3/033017)

New Journal of Physics
The open-access journal for physics

Plasmon damping below the Landau regime: the role of defects in epitaxial graphene

T Langer[1,2], J Baringhaus[1], H Pfnür[1], H W Schumacher[2] and C Tegenkamp[1,3]

[1] Institut für Festkörperphysik, Leibniz Universität Hannover, Appelstrasse 2, D-30167 Hannover, Germany
[2] Physikalisch-Technische Bundesanstalt, Bundesallee 100, D-38116 Braunschweig, Germany
E-mail: tegenkamp@fkp.uni-hannover.de

New Journal of Physics **12** (2010) 033017 (12pp)
Received 2 October 2009
Published 11 March 2010
Online at http://www.njp.org/
doi:10.1088/1367-2630/12/3/033017

Abstract. The sheet plasmon in epitaxially grown graphene layers on SiC(0001) and the influence of surface roughness have been investigated in detail by means of low-energy electron diffraction (LEED) and electron energy loss spectroscopy (EELS). We show that the existence of steps or grain boundaries in this epitaxial system is a source of strong damping, while the dispersion is rather insensitive to defects. To the first order, the lifetime of the plasmons was found to be proportional to the average terrace length and to the plasmon wavelength. A possible reason for this surprisingly efficient plasmon damping may be the close coincidence of phase (and group) velocities of the plasmons (almost linear dispersion) with the Fermi velocity of the electrons. Therefore, uncorrelated defects like steps only have to act as a momentum source to effectively couple plasmons to the electron–hole continuum.

Contents

[3] Author to whom any correspondence should be addressed.

1. Introduction

Graphene, a planar sheet of sp^2-bonded carbon atoms crystallized in a honeycomb lattice, has attracted much interest during the last few years. The peculiar band structure provides a material with outstanding mechanical, optical and electrical properties, e.g. the observation of the half-integer quantum Hall effect (QHE) [1, 2].

Single-graphene layers showing these unique properties can be obtained by exfolation of graphite, decomposition of hydrocarbons on transition metal surfaces or sublimation of Si from SiC surfaces [1], [3–5]. The system allows us to apply many surface-sensitive techniques; hence, mesoscopic transport properties can be correlated with the atomic structure. Furthermore, gating of the electron density by adsorption (e.g. Bi [6] or F4-TCNQ [8, 18]) has been shown to be an alternative to the electrical gating by contacts. Well-orientated graphene layers can be grown on SiC(0001) surfaces upon annealing. This graphitization process itself has been analyzed in detail in the past, among others with LEED, ARPES (angle resolved photoemission spectroscopy) and EELS [9–11]. Most importantly, an interface layer with $(6\sqrt{3} \times 6\sqrt{3})$ (also called a buffer layer and in the following denoted by $(6\sqrt{3})$) symmetry is formed in between the stoichiometric, Si-terminated SiC(0001) surface and the first graphene layer. Most challenging in this context is the preparation of almost perfect templates.

The ideal system reveals a delicate sublattice symmetry, i.e. at the K-points the chemical potential intersects the bonding and the antibonding states originate from both sublattices A and B, respectively; thus, intravalley (back-)scattering is strongly suppressed. Very recently the QHE has been found in epitaxially grown graphene layers as well, and it was demonstrated that epitaxial graphene is even suitable as a quantum resistance standard [12, 13]. However, it was also shown that atomic-sized defects and grain boundaries in these films act as scatterers [14, 15], leading e.g. to spatial variations of the surface potential [16], broader features in photoemission spectra [17, 18] or of the Landau levels if an external magnetic field is applied [19]. Recent experiments have revealed that the film roughness, i.e. the grain and island sizes, can be varied over orders of magnitude by different treatments. While long-time annealing under ultrahigh vacuum (UHV) conditions results in the growth of graphene islands of only a few nanometers in width, fast annealing at high temperatures (1600–2000 °C) at ambient Ar pressures around 1 atm favors the growth of almost perfect layers on the micron scale [20–22]. The optimized procedures lead to a uniform desorption of Si, i.e. the desorption rate in the vicinity of steps is reduced.

Plasmon spectroscopy has been used recently to characterize the 2D electron gas of graphene [23]. Theoretically, several attempts have been made to calculate accurately the plasmon dispersion including inter- and intraband transitions, intra- and intervalley scattering and static and dynamic screening effects [25, 26]. Furthermore, it was found that the reduced phase space implies a significantly shorter lifetime of the plasmons compared to that in almost free 2D Fermi gases. As we will show in this paper, static defects also play a crucial role with respect to the lifetime of plasmons.

Little is known quantitatively about the influence of atomic-size defects on plasmonic properties. While for Ag granular films a localization in the form of Mie resonances has been found, no influence of the steps has been seen for the Ag-$\sqrt{3} \times \sqrt{3}$ phase on Si(111) [27]. Here Landau damping limits the resolution. On the contrary, in $DySi_2$ films on Si(111) [28] a miscut of only 1° leads to a full suppression of the dispersion, while on flat substrates an isotropic dispersion has been found. These few results may be taken as an indication of the

close relationship between band structure, dielectric response, local geometric structure and plasmonic properties.

The importance of atomic steps in epitaxial graphene layers will be emphasized in this paper. We will show that, in contrast to the 2D system with a parabolically dispersing band structure, the graphene plasmon can decay via single-particle excitations already before the classical Landau damping regime has been entered [25]. This decay channel is very effective. Since the plasmon and electron dispersions are similar in energy, but shifted in momentum, the presence of static defects, e.g. steps, is sufficient for providing the necessary momentum transfer.

2. Experimental setup

All measurements were performed under UHV conditions. The pressure during the growth process did not exceed 5×10^{-7} Pa. Temperatures were measured with an IR pyrometer (Impac, $\epsilon = 0.99$). As the substrate, Si-terminated 6H-SiC(0001) samples (n-doped, $\approx 10^{18}\,\mathrm{cm}^{-3}$ from SiCrystal AG) were used, which were etched by an *ex situ* procedure in a furnace of H_2 atmosphere in order to remove the residual roughness from polishing steps [29]. Alternatively, *in situ* etched samples have been used. These were prepared by evaporation of 2–3 ML of Si at $1\,\mathrm{ML\,min}^{-1}$ at 800 °C in order to remove the native oxide. For the samples prepared *ex situ,* we obtained, after degassing at 750 °C for 12 h, instantaneously a LEED pattern showing the Si-rich (3×3) and $(\sqrt{3} \times \sqrt{3})$ structures. Annealing to 950 °C for 15 min leads to sublimation of Si and the formation of a C-rich $(6\sqrt{3} \times 6\sqrt{3})$ in coexistence with $(\sqrt{3} \times \sqrt{3})$, the precursor state for the buffer layer. Heating the sample further results first in the growth of the buffer layer. Graphene layers were finally grown on the buffer layer at higher annealing temperatures (1200 °C, figure 1(a)). For an exact thickness calibration for our setup, spot profile analysis of low-energy electron diffraction (SPA-LEED) and x-ray photoelectron spectroscopy (XPS) studies have been performed and correlated with results from electron energy loss spectroscopy (EELS) [11]. It should be emphasized here that graphene has been grown at high temperature in UHV, i.e. the graphene film is rough on a mesoscopic scale. The plasmons within the graphene layers were monitored by using a high-resolution electron loss spectrometer used as an electron source and detector of a low-energy electron diffraction (LEED) system. This system guarantees simultaneously a high energy and momentum ($k_{||}$) resolution [30] (the specular angle with respect to the surface normal is 6°, the maximal off-specular angle is 11°). Typical operating parameters were 25 meV energy resolution at a $k_{||}$ resolution of $1.3 \times 10^{-2}\,\text{Å}^{-1}$ in the energy range between 15 and 70 eV. The (elastic) k-resolution is judged from the minimal full-width at half-maximum (FWHM) of the (00)-reflex using well-prepared Si(111) surfaces.

3. Results and discussion

We first report on a quantitative analysis of roughness found for graphene films grown on differently treated SiC(0001) substrates. By both varying the initial step density of the substrate and the annealing time upon graphitization, the average terrace width can be varied between 10 and 150 nm. As the EEL-spectroscopy averages of many graphene grains, the roughness has been determined by means of SPA-LEED. In the second part (3.2), plasmonic losses within these films and their correlation with film roughness will be shown. In particular, the influence of the in-plane roughness will be discussed.

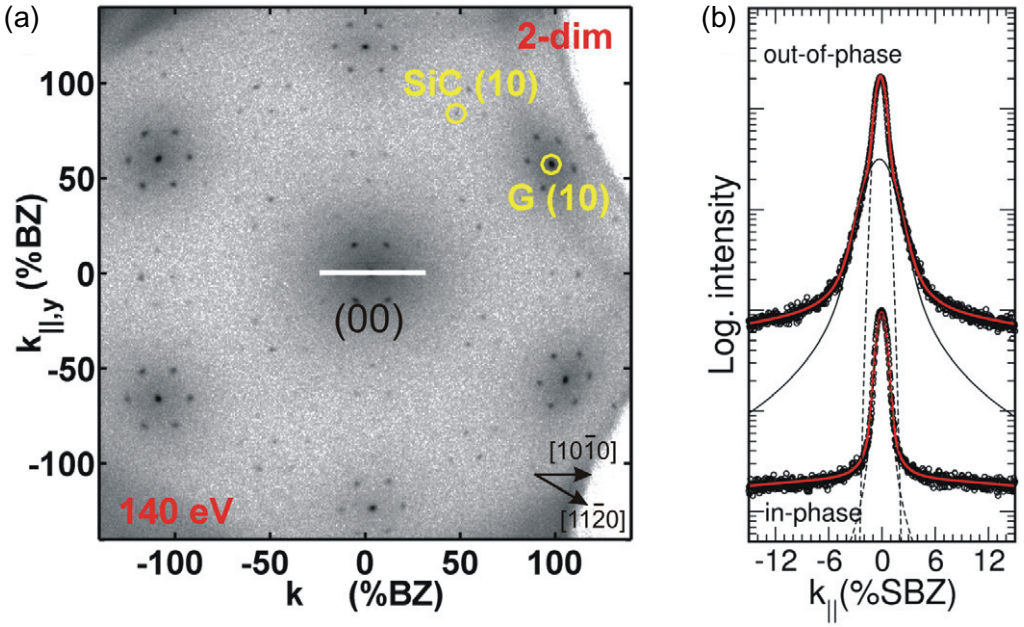

Figure 1. (a) 2D-LEED pattern of 1 ML graphene grown on H-etched SiC(0001). In order to quantify the roughness line scans, shown in (b), have been taken along the direction marked by the line. SiC(10) and G(10) denote first-order diffraction spots of the substrate and of graphene, respectively. (b) The line scans were taken at 130 and 155 eV corresponding to an in-phase ($S = 6$) and out-of-phase ($S = 6.5$) condition, respectively. In order to highlight the roughness, i.e. the shoulder (thin solid line) appearing in the upper curve, graphene grown on Si-etched samples has been taken. For better visibility, the background is not shown and the profiles are shifted.

3.1. The roughness of graphene layers

Well-oriented graphene layers can be grown on top of a buffer layer on SiC(0001) by heating the sample to high temperatures. Around 1200 °C, a carbon-rich phase remains forming the sp^2-hybridized carbon layer. The LEED pattern of a 1 ML graphene film grown on SiC(0001) is shown in figure 1(a). Owing to the lattice mismatch, the graphene film is rotated by 30° with respect to the substrate. According to first-principles calculations [31], the broken π-bonds within the buffer layer induce a strong potential modulation that appears in the form of a (6×6) reconstruction in LEED around each integer diffraction spot. Although this reconstruction is the dominant signature in LEED and STM [32], the $(6\sqrt{3})$-symmetry is preserved and has been seen in our recently performed high-resolution SPA-LEED study [11].

Figure 1(b) shows line scans taken along the [10$\bar{1}$0]-direction through the (00)-spot. From the lower curve recorded at an in-phase condition (electron energy $E = 130$ eV), i.e. where the scattering is by definition not sensitive to atomic steps on the substrate, only the transfer width of the SPA-LEED instrument limits the FWHM to 0.5% SBZ (surface Brillouin zone; $100\%\ \mathrm{SBZ} = 2\pi/a_{\mathrm{SiC}} \cdot \cos 30°$), which corresponds to approximately 250 nm. At an out-of-phase condition, on the contrary, the diffraction spots broaden; hence, the roughness is related

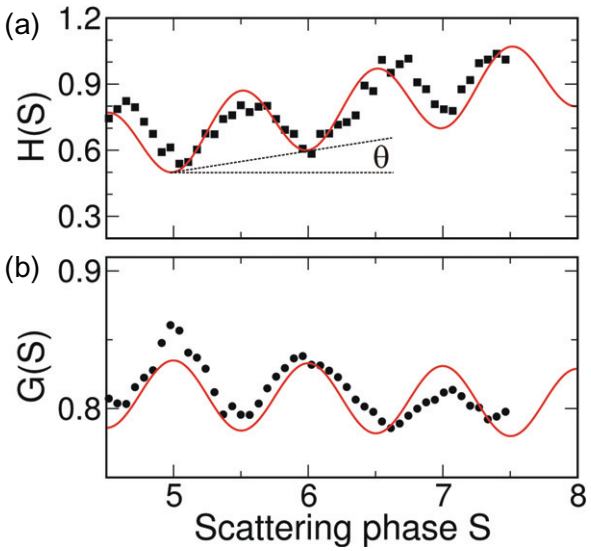

Figure 2. $H(S)$ (a) and $G(S)$ (b) of 1 ML graphene grown on H-etched SiC(0001) samples, from which the lateral and vertical roughness can be deduced within the transfer width of the LEED system. The scattering phases are given with respect to graphene single steps. Solid lines represent best fits according to [35]. For details see the text.

to the FWHM and the redistribution of the intensity, as shown exemplarily with the upper curve in figure 1(b) recorded at the electron energy of $E = 155$ eV ($S = 6.5$). Scattering conditions have been calculated with respect to graphene steps of mono-atomic height (see below) and the whole profiles can be accurately fitted with Gaussian functions for the central peak. The FWHM of the shoulder, fitted by Lorentzian-type functions, is around 5% SBZ, i.e. the average terrace length is only 80 graphene lattice sites (240 Å) [33].

In order to quantify the lateral and vertical roughness on a mesoscopic scale, which is also the characteristic length scale for plasmons, so-called $H(S)$- and $G(S)$-analyses have been performed, respectively. If multiple scattering processes are neglected, the variation of the FWHM of the shoulder in the diffraction profiles versus the scattering phase S (called $H(S)$, shown in figure 2(a)) provides information about the average terrace width Γ and the tilt angle (θ) due to mosaics. According to [35, 36], the FWHM varies as $4(1 - \cos(2\pi S))/\Gamma + \theta S$ in the presence of a certain step density $1/\Gamma$ within the transfer width of the instrument. The fitting of the data over a wide energy range, shown as a solid line in figure 2(a) for 1 ML graphene, reveals a small tilt of $\pm 0.02^\circ$ with respect to the surface normal, possibly induced during polishing of the sample, and an average terrace length of 75 nm. Almost perfect agreement of the in-phase and out-of-phase conditions, which are measured with high precision, is obtained if a step height of 3.2 Å is assumed, which is close to the step height in graphite. The contraction of 0.15 Å is most likely induced by a residual interaction between the buffer and graphene layers. The fact that the $H(S)$ curve oscillates with the graphene step height points unambiguously toward a non-uniformly grown graphene film. As in our experiments rather long annealing cycles (30 min in UHV) have been performed, preferentially desorption of Si from step sites takes place; thus fractions of bi- and even trilayer graphene are present. A similar growth has been found recently by LEEM [20].

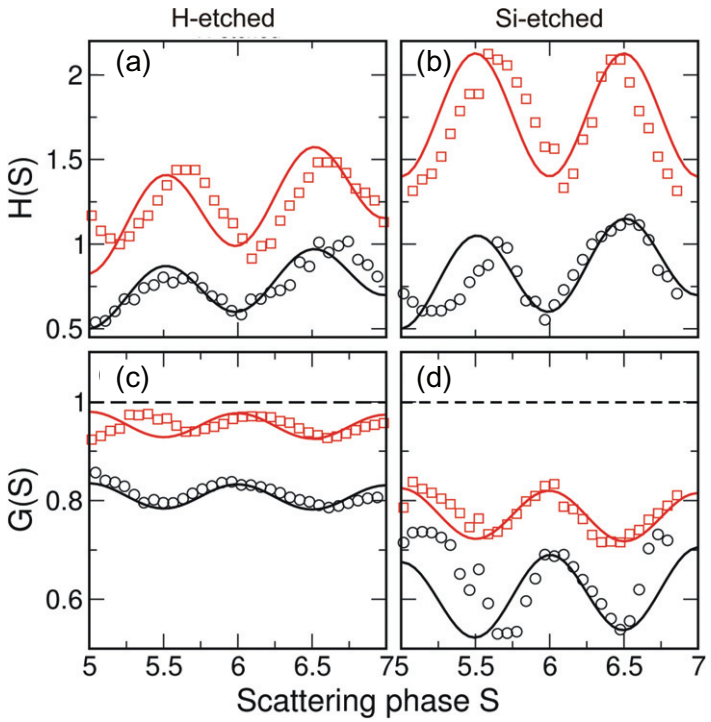

Figure 3. $H(S)$ (a, b) and $G(S)$ (c, d) curves of 1 ML (circles) and 2 ML (squares) thick graphene layers grown on H-etched (a, c) and Si-etched (b, d) SiC(0001) samples. Solid lines represent best fits to the experiment assuming only graphene steps and a bimodal height distribution.

The corrugation of the graphene film is obtained from the $G(S)$-curve, i.e. the ratio of the integral intensity of the central peak with respect to the total intensity as a function of the scattering phase. Figure 2(b) shows the $G(S)$ curve of a 1 ML graphene film grown on H-etched SiC(0001) samples. The curve is determined only by the vertical roughness including layer relaxation. For instance, an ideally smooth surface would yield $G(S) = 1$ irrespective of the electron energy (cf the dashed lines in figures 3(c) and (d)). On the contrary, for a rough surface, for instance, a two-level system where the surface area of the first and second layers are the same, $G(S)$ vanishes completely at any out-of-phase condition. Thus, a $G(S)$-curve provides information about the distribution of the layers as well.

In the particular case shown in figure 2(b) for the 1 ML graphene layer, the rms roughness is 4 Å. Although this rms value is comparably low, the corrugation of almost perfect graphene layers grown in an Ar atmosphere reveals only 0.2 Å [22]. From the amplitude of the $G(S)$ curve, the occupancy of the second layer was determined to be less than 10%. Furthermore, all $G(S)$ curves shown here are described reasonably by a single cosine function, which is characteristic of a two-level system [35]. Both the relative occurrence of the bilayer fraction and, hence, the increased rms roughness fully support the results obtained by LEEM measurements [20]. The gradual damping of the oscillations as the scattering phase increases is explained by the variation of the layer distances within this hetero-film structure [37] and supports the finding of layer relaxation for graphene layers grown on SiC templates.

The best agreement with the $G(S)$ and $H(S)$ oscillations has been obtained assuming graphene steps of single atomic height. As we have not seen pronounced phase shifts induced by SiC steps ($d = 2.54$ Å), the initial SiC step density seems to be reduced further by the Si-sublimation and the graphene growth process. Recent STM studies have shown that SiC steps tend to be overgrown. For instance, if the bilayer grows on the lower terrace, the corrugation to the monolayer graphene on the upper terrace is as low as 0.7 Å. Furthermore, the graphene grows in a bottom-up manner; hence, the topmost graphene film is continuous across the boundaries between mono- and bilayer regions [34].

As a consequence of the sp^2-hybridization, graphene can overgrow in carpet-like mode steps [38]; hence, the step density within the graphene layer is usually lower than for the substrate itself. However, as seen above, the process is limited by the initial step concentration of the SiC samples. In order to demonstrate the residual impact of the substrate roughness, figure 3 summarizes $H(S)$- and $G(S)$-curves for one and two monolayer graphene on H-etched and Si-etched samples, respectively. The comparison of figures 3(a) and (b) reveals that the lateral roughness of graphene on Si-etched samples is typically by a factor of two higher. The case shown in figure 3(b) has an average terrace length of 40 nm. This influences sensitively the lifetime of plasmonic excitations as we will show below.

Furthermore, the roughness of the nominally two-monolayer graphene compared to only one (the circles in figure 3) is slightly increased as well. The relative increase of the lateral roughness depends nearly not on the treatment of the substrate before the graphitization process; however, the mosaic angle is slightly enlarged for the graphene layers grown on Si-etched samples, i.e. the high-temperature steps during the H-etching reduces, to some extent, also bulk defects.

The resulting roughness of the graphene layer depends strongly on the initial step concentration. As the Si-etched samples have a higher step density, the bilayer fraction should be larger. This is reflected directly by the larger amplitude of the oscillations in the $G(S)$ curve shown in figure 3(d) compared to figure 3(c). The bilayer fraction is close to 20% and, hence, the rms roughness is increased as well (8 Å). Solid lines represent best fits assuming only a bimodal layer height distribution. Although this model still reasonably described the roughness of the closed graphene film, deviations also become obvious as the SiC step roughness and the graphene layer thickness increase. Compared to other systems, the graphene system exhibits an extraordinary smoothness, but still the remaining roughness has a large impact on the lifetime of plasmonic losses within these layers.

3.2. Spectroscopy of plasmons

In order to characterize the electronic properties of these films, plasmons have been studied by means of EELS. Before the influence of the roughness is discussed, first the spectra obtained during the graphitization process and of an 1 ML graphene itself will be presented.

Figure 4(a) shows an EELS sequence (20 eV electron energy) before and after graphitization. While the lowest curve is characteristic of the clean SiC surface, the other shows the graphene layer grown on top (for calibration, see [11]). The loss peak around 150 meV can be attributed to the Fuchs–Kliewer (FK) mode of the graphene film [23, 24] or to the SiC substrate itself, as a comparison with the lowest spectrum, showing also higher FK modes, suggests. Details of energetic shifts of the FK phonons of differently reconstructed SiC surfaces can be found in [39].

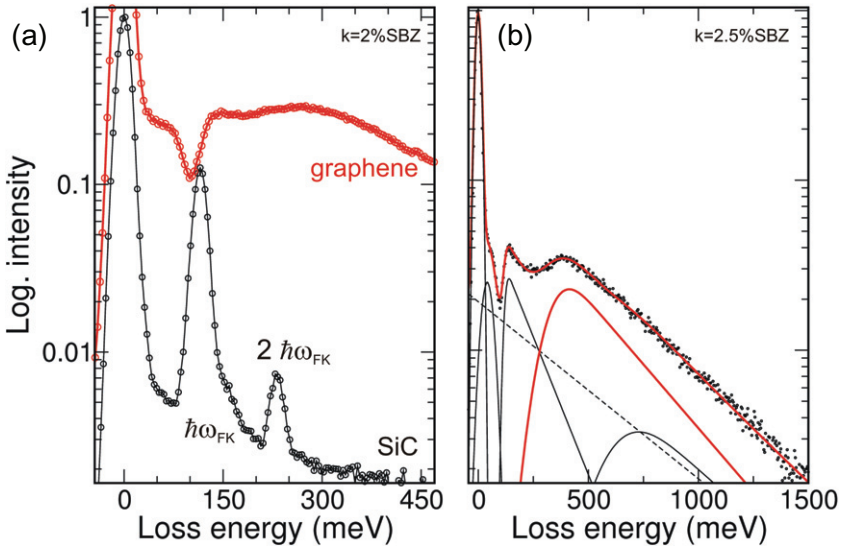

Figure 4. (a) EEL spectra of the SiC surface before and after graphitization. The primary electron energy was 20 eV. In order to separate the plasmonic loss from the FK mode around 150 meV, the spectra have been taken at an off-specular scattering condition corresponding to the momentum transfer values, k, indicated at the top. The peaks are shifted for better visibility. (b) EEL spectrum of 1 ML graphene grown on an H-etched SiC(0001) sample together with the composition of the spectrum from loss peaks due to phonons (black thin lines to the left) and plasmons (red thin line). The dashed line denotes the contribution of the Drude background.

The broad peak around 300 meV appears only for the graphene-like phases and is attributed to the 2D sheet plasmon [23]. In order to separate it from the barely dispersing phonon modes, the spectra were taken at 0.047 Å^{-1} (2% SBZ). The FWHM of the loss peak is not limited by the resolution of the instrument, which was around 25 meV, and it is also not limited by the finite k-space resolution (see below). The origin of the peak around 70 meV, which neither disperses in the considered wave vector range (0–10% SBZ), has not yet been clarified. However, it was recently assigned to a low-energy π-plasmon, since it was found for graphitic surfaces as well [23, 24]. This loss can be clearly resolved at first after a complete graphene layer is grown, while for the buffer layer (not shown) the peak appears strongly damped. This behavior can be interpreted as the result of a stepwise metallization and supports our finding in a former study [11]. Nonetheless, it should be mentioned here that the assignment of the losses around 70 meV (low-energy π-plasmon) and 150 meV (FK phonon) is controversially discussed. High-resolution EELS measurements have shown that both peaks disperse slightly and that they have to be assigned to the so-called ω_- and ω_+ losses due to an enhanced plasmon–phonon coupling [40]. However, our conclusions in the following are not affected by this.

In order to determine accurately the peak positions and the FWHM of the plasmon losses, the spectra have been fitted, as exemplarily shown in figure 4(b) for 1 ML graphene layer grown on an H-etched SiC(0001) sample at $k = 0.06$ Å^{-1} (2.5% SBZ). All spectra could reasonably be described assuming the characteristic phonon and plasmon losses just mentioned. The individual losses were modeled using exponentially modified Gaussian (EMG) functions,

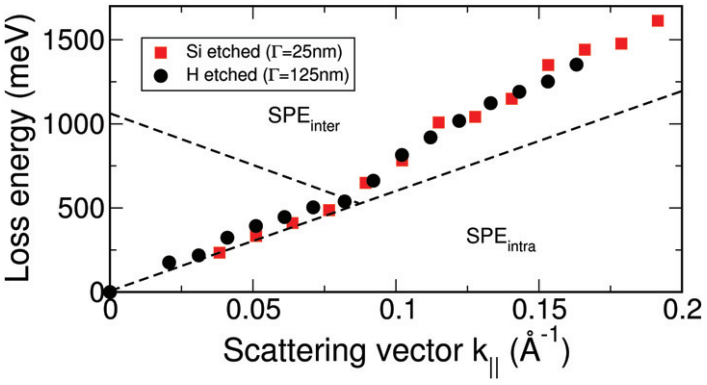

Figure 5. Plasmon dispersion of 1 ML graphene grown on H- and Si-etched samples. Although the average terrace width differs by a factor of 5, the dispersion is rather the same. SPE_{intra} and SPE_{inter} denote the regime of single particle (electron–hole) excitations by intra- and interband transitions.

which are motivated by the extremely slowly decaying background with increasing loss energy. A similar behavior, where the whole background was described by a single error function, was found by Palmer *et al* [41] for graphitic surfaces accounting for the half-metallic-like band structure. It should be noted that the asymmetry factor of the EMG depends on the samples. For instance, the spectra discussed in context with figure 6(a) could be described almost by pure Gaussians. Furthermore, taking into account a second loss feature, whose loss energy is approximately twice as large as the dominant one and is attributed to the excitation of a second plasmon quantum or a multimode excitation (multiplasmons), the slowly decaying tail in figure 4 can be consistently fitted.

For these clearly identifiable loss peaks, the loss energies and the FWHMs have been determined, focusing on the low-energy sheet plasmon. Figure 5 shows the dispersion of this plasmon in a graphene monolayer grown on Si- and H-etched SiC samples. Although the lateral roughness differs by a factor of 5, the dispersion is the same, i.e. by inference the band structure in the regions of perfect graphene is unaffected by the defects. In agreement with previous studies [23], the plasmon dispersion shows specific signatures: in the long wavelength limit up to 0.08 $Å^{-1}$ the dispersion is rather linear, in agreement with calculations based on the random phase approximation [25]. Secondly, for $k > 0.1\ Å^{-1}$ the dispersion shifts to higher plasmon energies. This is a result of strong correlation between the electrons in this 2D system [42], preventing the system from entering the Landau damping regime denoted by SPE_{intra} in figure 5. Both SPE regimes due to intra- and interband excitations sketched in figure 5 rely on a Fermi energy of 520 meV. As a consequence of unsaturated bonds at the interface, this value reflects a realistic electron concentration and is close to the values found by ARPES [43]. The corresponding Fermi wavevector of 0.08 $Å^{-1}$ is identical to the one found in [23]. As is obvious from figure 5, the linear dispersion reveals a plasmon velocity that is almost identical to the Fermi velocity of the electrons in this highly correlated system ($\approx 1 \times 10^6\ m\,s^{-1}$). As we will see in the following, this has a dramatic consequence for the lifetime of plasmonic excitations in the presence of defects.

Compared to other loss spectra, the extraordinary broad loss peak seems to be a characteristic signature of the graphene films on SiC substrates [23]. Figure 6(a) shows

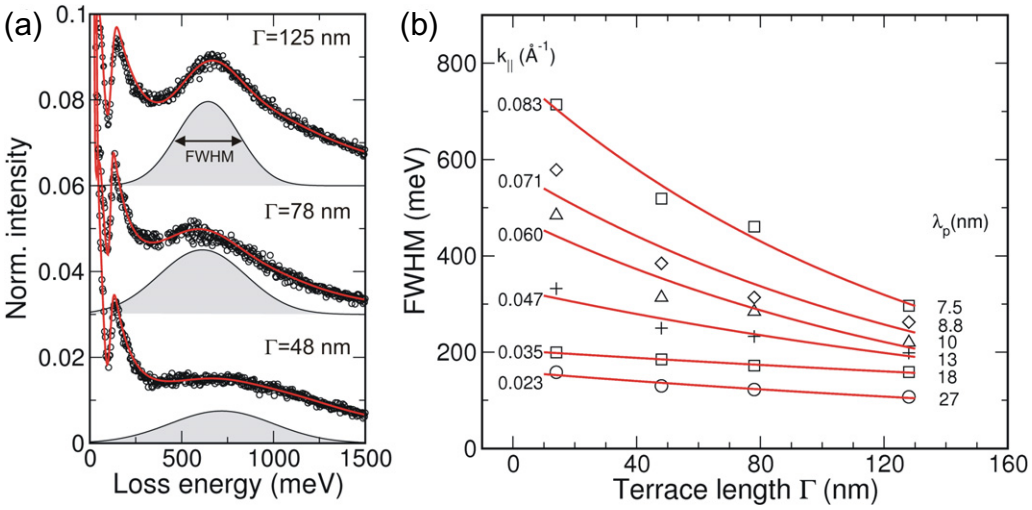

Figure 6. (a) EEL spectra of 1 ML graphene (shifted for better visibility) taken at $k = 0.09$ Å^{-1} (lower curve at 0.094 Å^{-1}). Only the plasmon peak is highlighted in order to illustrate the broadening as the average terrace length shrinks. The lower spectrum was taken from graphene grown on Si-etched samples. (b) FWHM of the plasmon loss versus the terrace length Γ as a function of the plasmon wavelength $\lambda_P = 2\pi/k_{||}$. For further details see the text.

exemplarily three EEL spectra taken around 4% SBZ (0.09 Å^{-1}) on graphene with different average terrace lengths, as denoted in the graph. The shaded peak, showing the contribution of the sheet plasmon, becomes broader as the roughness of the graphene layer increases. This broadening is not given by the instrument.

All EELS measurements shown here were performed at 20 eV, as this energy has revealed a satisfactory signal-to-noise ratio. However, this energy is close to an out-of-phase condition, i.e. the energy resolution due to k-space limitation depends on the roughness of the surface itself. For instance, from the roughness analysis, we have seen that the FWHM of the (00)-diffraction spot taken on the H-etched samples at an out-of-phase condition is typically around 1% SBZ (0.023 Å^{-1}, cf with figure 3). According to the plasmon dispersion, the energy resolution is therefore restricted in this case to 125 meV. This is considered when the FWHM of the plasmons is discussed. Furthermore, only the damping of the plasmons up to 0.1 Å^{-1} (cf with figure 5) is discussed in the following. For higher scattering momenta, interband transitions are energetically favored, as the plasmons enter this *classical* Landau damping. A detailed analysis of the FWHM for different plasmon wavelengths λ_P is shown in figure 6(b) obtained on four graphene substrates that differ in their average terrace length Γ by one order of magnitude. The FWHM dependency obtained for the longest plasmon wavelength that could be measured ($\lambda_P = 27$ nm) has been taken as the instrument function and is subtracted from the data shown.

The plot reveals two interesting pieces of information, which are helpful to elucidate the role of atomic-sized steps: for a fixed plasmon wavelength, the FWHM decreases as the terrace size increases. Furthermore, the analysis has revealed that the lifetime is almost inversely proportional to the step concentration (Γ), i.e. steps lead to a strong plasmon damping. Secondly, for a given roughness, the FWHM increases as λ_P decreases and the lifetime is almost proportional to the plasmon wavelength λ_P. As in any transport experiment, the cross section for

scattering increases when the wavelength and characteristic length scale of the defect become comparable.

The FWHM of the plasmons in graphene is larger than that of 2D systems with parabolically dispersing electronic band structures. The results have shown that already below the Landau threshold, defined by the band structure, the broadening is significant. Although graphene is a highly correlated system, this cannot explain the strong damping solely. In 2D systems like Ag/Si(111), the broadening due to exchange correlation is of the order of less than 1% of the relative width of the plasmon peak [44, 45]. As we have seen above, the dispersions for both the collective and single electron excitations are almost identical. At least the group velocities in between $0.03\,\text{Å}^{-1} < k < 0.08\,\text{Å}^{-1}$ are within the precision of measurements the same. In this regime, plasmons can dissipate without gaining energy. Uncorrelated defects, e.g. steps, can act as momentum sources. For the shortest terrace length investigated here, the step concentration is close to 2% of a monolayer; however, as the dispersion is not changed by the step density, it is reasonable to assume that steps and grain boundaries provide dispersionless states. For other 2D systems, the plasmon dispersion is proportional to $\sqrt{k}$, while the SPE border is $\sim k^2$; thus, the decay of plasmons is only possible when both energy and momentum are exchanged during the scattering of the plasmon. As a result, the strong damping of plasmons is a unique property of graphene.

4. Summary and outlook

In summary, we have presented a comprehensive study of the lifetime of collective excitations in epitaxially grown graphene layers. The roughness of these films has been changed between 14 and 125 nm of the average terrace length using SiC substrates. The spectroscopy of the plasmons has revealed that steps do not change the graphene band structure significantly, as the plasmon dispersion is insensitive to these defects. On the contrary, the lifetime of these collective excitations is strongly reduced by steps. In particular, it was found that the lifetime is proportional to the step density and plasmon wavelength ($\tau \sim \lambda_P \cdot \Gamma$). As the plasmon dispersion is linear in the long-wavelength range and reveals almost the same group velocity as the band structure, steps can effectively mediate the momentum transfer, making the plasmon decay more effective. Toward the use of graphene in plasmonics, i.e. the transport of plasmons, the needs with respect to the step density will be rather demanding. However, in order to quantify the transmission of these line defects, further studies in which the primary electron energy is systematically varied have to be performed.

References

[1] Novoselov K S, Geim A K, Morozov S V, Jiang D, Zhang Y, Dubonos S V, Grigorieva I V and Firsov A A 2004 *Science* **306** 666
[2] Geim A K and Novoselov K S 2007 *Nat. Mater.* **6** 183
[3] Coraux J, N'Diaye A T, Busse C and Michely T 2008 *Nano Lett.* **8** 565
[4] Sutter P W, Flege J I and Sutter E A 2008 *Nat. Mater.* **7** 406
[5] Ohta T, Bostwick A, Seyller Th, Horn K and Rotenberg E 2006 *Science* **313** 951
[6] Gierz I, Riedl C, Starke U, Ast R and Kern K 2008 *Nano Lett.* **8** 4603
[7] Zhou S Y, Siegel D A, Fedorov A V and Lanzara A 2008 *Phys. Rev. Lett.* **101** 086402
[8] Chen W, Chen S, Qi D C, Gao X Y and Wee A T S 2007 *J. Am. Chem. Soc.* **129** 10418

[9] Riedl C, Starke U, Bernhardt J, Franke M and Heinz K 2007 *Phys. Rev.* B **76** 245406
[10] Emtsev K V, Speck F, Seyller Th, Ley L and Riley J D 2008 *Phys. Rev.* B **77** 155303
[11] Langer T, Schumacher H W, Pfnür H and Tegenkamp C 2009 *Appl. Phys. Lett.* **94** 112106
[12] Jobst J, Waldmann D, Speck F, Hirner R, Maude D K, Seyller Th and Weber H B 2009 arXiv:0908.1900v1 [cond-mat]
[13] Tzalenchuk A, Lara-Avila S, Kalaboukhov A, Paolillo S, Syväjärvi M, Yakimova R, Kazakova O, Janssen T J B M, Fal'ko V and Kubatkin S 2010 *Nature Nanotech.* **5** 186–9
[14] Rutter G M, Crain J N, Guisinger N P, Li T, First P N and Stroscio J A 2007 *Science* **317** 219
[15] Chen J H, Cullen W G, Jang C, Fuhrer M S and Williams E D 2009 *Phys. Rev. Lett.* **102** 236805
[16] Filleter T, Emtsev K V, Seyller Th and Bennewitz R 2008 *Appl. Phys. Lett.* **93** 133117
[17] Rotenberg E, Bostwick A, Ohta T, McChesney J L, Seyller T and Horn K 2008 *Nat. Mater.* **7** 258
[18] Zhou S Y, Siegel D A, Fedorov A V, Gabaly El F, Schmid A K, Castro Neto A H, Lee D H and Lanzara A 2008 *Nat. Mater.* **7** 259
[19] Miller D L, Kubista K D, Rutter G M, Ruan M, de Heer W A, First P N and Stroscio J A 2009 *Science* **324** 924
[20] Ohta T, El Gabaly F, Bostwick A, McChesney J L, Emtsev K V, Schmid A K, Seyller Th, Horn K and Rotenberg E 2008 *New J. Phys.* **10** 023034
[21] Virojanadara C, Syväjärvi M, Yakimova R and Johannson L I 2008 *Phys. Rev.* B **78** 245403
[22] Virojanadara C, Yakimova R, Osiecki J R, Syväjärvi M, Uhrberg R I G, Johansson L I and Zakharov A A 2008 *Surf. Sci.* **603** L87
[23] Liu Y, Willis R F, Emstev K V and Seyller Th 2008 *Phys. Rev.* B **78** 201403
[24] Angot T, Portail M, Forbeaux I and Layet J M 2002 *Surf. Sci.* **502–3** 81
[25] Hwang E H and Das Sarma S 2007 *Phys. Rev.* B **75** 205418
[26] Hill A, Mikhailov A and Ziegler K 2009 *Eur. Phys. Lett.* **87** 27005
[27] Nagao T, Hildebrandt T, Henzler M and Hasegawa S 2001 *Phys. Rev. Lett.* **86** 5747
[28] Rugeramigabo E P, Nagao T and Pfnür H 2008 *Phys. Rev.* B **78** 155402
[29] Emtsev K V *et al* 2009 *Nat. Mater.* **8** 203
[30] Claus H, Büssenschütt A and Henzler M 1992 *Rev. Sci. Instrum.* **4** 2195
[31] Kim S, Ihm J, Choi H J and Son Y W 2008 *Phys. Rev. Lett.* **100** 176802
[32] Vitali L, Riedl C, Ohmann R, Brihuega I, Starke U and Kern K 2008 *Surf. Sci. Lett.* **602** L127
[33] Henzler M 1997 *Surf. Rev. Lett.* **4** 489
[34] Huang H, Chen W, Chen S and Wee A T S 2008 *ASC Nano* **2** 2513
[35] Horn-von Hoegen M 1999 *Z. Kristallogr.* **214** 591
[36] Lu T M and Lagally M 1982 *Surf. Sci.* **120** 47
[37] Al-Falou A A, Kammler M and Horn-von Hoegen M 2005 *Europhys. Lett.* **69** 570
[38] Seyller Th *et al* 2006 *Surf. Sci.* **600** 3906
[39] Balster T, Tautz S F, Polyakov V, Ibach H, Sloboshanin S, Öttking R and Schaefer J 2006 *Surf. Sci.* **600** 2886
[40] Schaefer J 2009 private communication
[41] Palmer R E, Annett J F and Willis R F 1987 *Phys. Rev. Lett.* **58** 2490
[42] Stern F 1967 *Phys. Rev. Lett.* **18** 546
[43] Bostwick A, Ohta T, Seyller T, Horn K and Rotenberg E 2007 *Nat. Phys.* **3** 36
[44] Holas A and Singwi K S 1989 *Phys. Rev.* B **40** 158
[45] Nazarov V U, Nishigaki S and Nagao T 2002 *Phys. Rev.* B **66** 092301